Letter

Zoology of non-Hermitian spectra and their graph topology

Tommy Tai [1,2,3,*] and Ching Hua Lee [3,†]

[1] *Department of Physics, Massachusetts Institute of Technology, 77 Massachusetts Ave, Cambridge, Massachusetts 02139, USA*
[2] *Cavendish Laboratory, University of Cambridge, JJ Thomson Ave, Cambridge CB3 0HE, United Kingdom*
[3] *Department of Physics, National University of Singapore, Singapore 117542*

(Received 13 February 2022; revised 17 May 2023; accepted 18 May 2023; published 14 June 2023)

We uncover the very rich graph topology of generic bounded non-Hermitian spectra, distinct from the topology of conventional band invariants and complex spectral winding. The graph configuration of complex spectra are characterized by the algebraic structures of their corresponding energy dispersions, drawing new intimate links between combinatorial graph theory, algebraic geometry, and non-Hermitian band topology. Spectral graphs that are conformally related belong to the same equivalence class, and are characterized by emergent symmetries not necessarily present in the physical Hamiltonian. The simplest class encompasses well-known examples such as the Hatano-Nelson and non-Hermitian SSH models, while more sophisticated classes represent novel multicomponent models with interesting spectral graphs resembling stars, flowers, and insects. With recent rapid advancements in metamaterials, ultracold atomic lattices, and quantum circuits, it is now feasible to not only experimentally realize such esoteric spectra, but also investigate the non-Hermitian flat bands and anomalous responses straddling transitions between different spectral graph topologies.

DOI: 10.1103/PhysRevB.107.L220301

Introduction. Topological classification plays an indispensable role in modern condensed matter physics, identifying the intrinsic robustness in ionic compounds [1,2] and engineered metamaterial platforms such as photonic [3–12], mechanical [13–19], and electrical setups [20–35].

Conventionally, topological classification pertains to the classification of eigenstate windings, specifically the topology of the mapping between the Brillouin zone (BZ) and the target state space. This notion of topology underscores all topological insulators [36–43], higher-order topological insulators [44–48], and indeed practically all Hermitian topological lattices, symmetry-protected or otherwise. The accompanying topological invariant is connected to a quantized observable such as Hall conductivity [36–38,49–51],[1] which is as such protected from continuously degrading.

In this work, we focus on a different type of topology, namely the spectral graph topology, which is found to be far more intricate and exotic than conventional $\mathbb{Z}$ or $\mathbb{Z}_2$ topological [37,52] classes. As presented in Fig 1(c), the energy spectra of various bounded non-Hermitian lattices take on a kaleidoscope of interesting shapes resembling stars, flowers, or even insects, consisting of lines or curves that connect spectral vertices in all imaginable ways. Compared to eigenstate [Fig. 1(a)] or exceptional point [Fig. 1(b)] [53–65] topology, which are represented by homotopy windings, the planar graph topology of these non-Hermitian spectra can be much more sophisticated, encoding arbitrarily complicated connectivity structures. Indeed, the number of distinct planar graphs with $\mathcal{N}$ branching vertices scales rapidly as [66] $\sim\mathcal{N}^{-7/2}\gamma^{\mathcal{N}}\mathcal{N}!$ with $\gamma\approx 27.27$, and no single topological invariant can unambiguously distinguish between two different graphs.

Just like how conventional eigenstate topology manifests as linear response quantization, topological transitions between different spectral graphs physically manifest as linear response kinks. This is because different parts of the eigenstates mix abruptly when at transitions between different

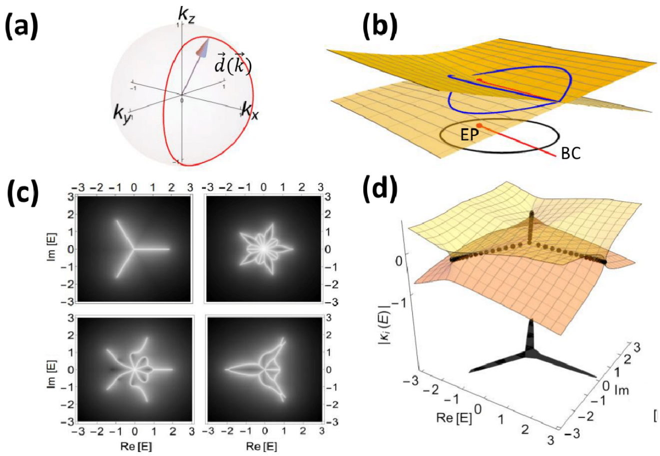

FIG. 1. Conventionally, topology typically refers to the winding number either (a) in the state space or (b) around the exceptional point (EP) branch cut (BC). (c) This work uncovers the very intricate graph topology of the spectra of non-Hermitian bounded lattices, which originates from (d) the intersections of its inverse skin depth solution surfaces $|\kappa_i(E)|$.

[*] ytt26@cam.ac.uk
[†] phylch@nus.edu.sg
[1] However, see Ref. [150], which concerns a quantized measurable quantity for winding in the energy plane.

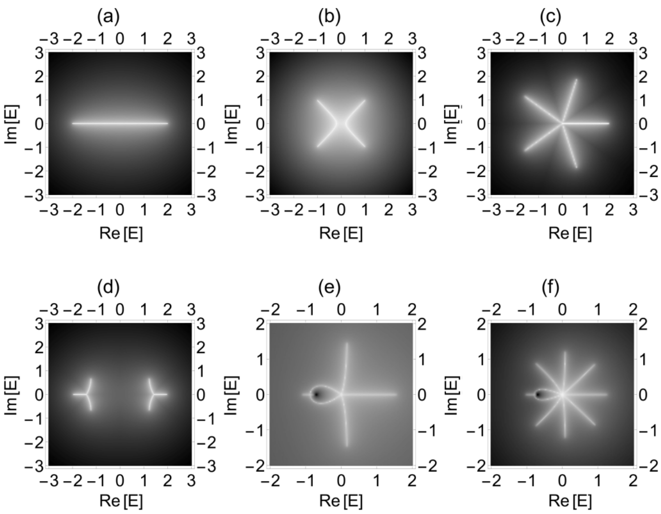

FIG. 2. Elementary illustrative OBC spectral graphs $\bar{E}$: (a) real spectral line segment of the Hatano-Nelson model; (b) hyperbola spectral segments of the non-Hermitian SSH model with $|\mu| > |t|$; (c) five-pronged star for $F(E) = E$ and $a = 3$, $b = 2$; (d) Two deformed three-stars from the OBC spectrum of $H^{2\text{-band}}_{2,1}$ with $a = 2$, $b = 1$, and $F(E) = 2 - E^2$; (e)–(f) Looped spectral graphs from Eq. (3), with (e) $G(E) = E^2 + 0.7E$, $F(E) = E^3$, and (f) $G(E) = E^4 + 0.7E^3$, $F(E) = E^6$.

graph configurations, resulting in enigmatic gapped marginal transitions with no Hermitian analog [67]. In the simplest cases, such transitions have also been associated with Berry curvature discontinuities [68]. Since real experimental setups are almost always finite and bounded, the requirement of open boundary conditions (OBCs) does not diminish the physical significance of spectral graph topology [69] (see also Refs. [26,68,70–90] therein).

Deep mathematical relationships exist between the spectral graph topology of a system and the algebrogeometric properties of its energy-momentum dispersion. As elaborated shortly, the dispersion can be written as a bivariate Laurent polynomial $P(E, z)$, where E and $z = e^{ik}$ are the energy and complex exponentiated momentum, respectively. In lattices with multiple components (bands) or hoppings, the OBC spectral graph quickly becomes very intricate,[2] and $P(E, z)$ becomes a fingerprint of the set of its possible graph topologies. This correspondence survives under conformal transformations in the complex energy, which is a vast group of symmetries tying together otherwise unrelated Hamiltonians. In charting out the classification table for distinct graph topologies, we also uncover emergent symmetries absent in the original Hamiltonian, leading to alternative avenues for engineering real non-Hermitian spectra beyond PT symmetry [28,91–98]

Spectral graphs from energy dispersions. Under OBCs, the spectrum of generic non-Hermitian lattices collapses into straight lines or curves [70,71,99] that join to form a planar graph made up of stars and loops [Figs. 1(c), 2(a)–2(f)]. To understand why, we first highlight the fundamental role played by the dispersion relation

$$P(E, z) = \mathrm{Det}[H(z) - E\,\mathbb{I}] = 0, \tag{1}$$

which is the characteristic polynomial of the Hamiltonian $H(z)$, $z = e^{ik}$. In an unbounded periodic crystal, the spectrum is simply the set of E satisfying $P(E, e^{ik}) = 0$ for real momenta $k \in [0, 2\pi)$. However, under OBCs, this is not the case since k no longer indexes the eigenstates due to broken translation symmetry. Yet, because the bulk is still translation invariant, any eigenstate must be composed of eigensolutions of Bloch-like form, characterized by complex instead of real momenta k. The imaginary part of the momentum $\mathrm{Im}(k)$ represents spatial decay rate (since $|e^{ikx}| \sim e^{-(\mathrm{Im}k)x}$), and is also known as the inverse skin depth [68,70–73,95,96,99–117].

In particular, for an eigenstate to satisfy OBCs, it must simultaneously vanish at both ends, and that requires it to be a superposition of degenerate eigensolutions with equal skin depths [69][3] As a consequence, the OBC spectrum consists[4] of the set of energies $E \in \{\bar{E}\}$ that satisfy $P(\bar{E}, z) = 0$, and which are simultaneously degenerate in both E and $\mathrm{Im}\,k = -\log|z|$.

Interpreted geometrically, these conditions imply that OBC eigenenergies must lie on a planar graph: On the complex E plane, solutions to $P(E, z) = 0$ that are degenerate in both E and $\mathrm{Im}\,k = -\log|z|$ can be visualized geometrically as the intersections of $\mathrm{Im}\,k$ surfaces. Intersections of two $\mathrm{Im}\,k$ surfaces trace out curves, i.e., graph edges, while intersections of three or more $\mathrm{Im}\,k$ surfaces produce branch points, i.e., spectral graph vertices [Fig. 1(d)]. Together, these intersection loci trace out a planar spectral graph on the complex plane. Note that if $P(E, z)$ is of degree p in z, there exist p surfaces of $\mathrm{Im}\,k$ everywhere due to the fundamental theorem of algebra [118]. Indeed, the OBC spectral graph depends solely on the algebraic form of $P(E, z)$; the exact form of the Hamiltonian $H(z)$ is inconsequential. This is actually already the case in Hermitian lattices; bulk bands are computed from the dispersion relation $P(E, z) = 0$, and not explicitly from $H(z)$ *per se*. What is unique and interesting in the non-Hermitian context is the key role played by $\mathrm{Im}\,k$ solution surfaces across the entire complex E plane, not just points satisfying $P(E, z) = 0$.

To understand how $P(E, z)$ determines the possible spectral graphs $\bar{E}$, we first mention two important symmetries that greatly simplify their distinct classification. First, all Hamiltonians related by a translation of imaginary momentum $H(k) \to H(k + i\kappa)$, i.e., real-space rescaling $c_x^\dagger \to c_x^\dagger e^{-\kappa x}$ possess [70] identical OBC spectra $\bar{E}$. This is because $\bar{E}$ depends on the intersections of $\mathrm{Im}\,k$ surfaces, which cannot change if all solution surfaces are translated by an equal amount κ. As such, all polynomials related by rescalings of z, i.e., $P(E, z) \to P(E, e^{-\kappa} z)$ correspond to the same set of

[2]The exact OBC spectrum quickly becomes analytically intractable, since, due to the Abel-Ruffini theorem, no generic analytic solution is possible for sufficiently high-order polynomials [151].

[3]If the decay rates are not equal, we are left with effectively one eigenstate in the thermodynamic limit, and the state wave function cannot vanish at both ends and satisfy OBCs.

[4]With the exception of a small number of isolated states protected by eigenstate topology, if any.

$\bar{E}$, allowing for the normalization of the coefficients of z (hopping amplitudes) without loss of generality.

Second, different $P(E,z)$ related by a conformal mapping of E possess OBC spectra $\bar{E}$ related by the same mapping, i.e., if $P'(E,z)=P(f(E),z)$, then $\bar{E}'=f(\bar{E})$ [69]. In other words, when classifying $P(E,z)$, one only needs to consider the simplest functional dependencies on E.

Elementary examples. To facilitate our spectral graph classification through $P(E,z)$, we first examine the few simplest examples with analytically known OBC spectra.

(i) $P(E,z)=F(E)-(z+z^{-1})$.

This simplest case can be written in the separable form $F(E)=z+z^{-1}$, where $F(E)$ is solely dependent on E, and the right-hand side depends only on z. It encompasses the two most well-known non-Hermitian lattice models: the Hatano-Nelson and non-Hermitian SSH models given by Refs. [74,75,100] $H_{\mathrm{HN}}(z)=uz+vz^{-1}$, and $H_{\mathrm{SSH}}(z)=(t-\mu+z)\sigma_+ +(t+\mu+z^{-1})\sigma_-$, respectively. For the single-component H_{HN}, the energy eigenequation is $E-(uz+vz^{-1})=0$, which can be rewritten as $P_{\mathrm{HN}}(E,z)=E/\sqrt{uv}-(z+z^{-1})=0$ after letting $z\to\sqrt{\frac{u}{v}}z$ and $F(E)=E_{\mathrm{HN}}/\sqrt{uv}$. For the two-component H_{SSH}, we have $E^2=(t-\mu+z)(t+\mu+z^{-1})=(t^2-\mu^2+1)+(t+\mu)z+(t-\mu)z^{-1}$, which can also be written as $P_{\mathrm{SSH}}=F_{\mathrm{SSH}}(E)-(z+z^{-1})$ upon letting $z\to z\sqrt{\frac{t+\mu}{t-\mu}}$ and defining $F_{\mathrm{SSH}}(E)=(E^2+\mu^2-t^2-1)/\sqrt{t^2-\mu^2}$.

Now, since $z+z^{-1}$ is invariant under $z\leftrightarrow z^{-1}$, it is doubly degenerate when $|z|=|e^{ik}|=1$. Thus the OBC spectrum $\bar{E}$ is just given by $F(\bar{E})=2\cos k$, $k\in\mathbb{R}$. For the Hatano-Nelson model, we thus have $\bar{E}_{\mathrm{HN}}=2\sqrt{uv}\cos k$, which is a real line interval when $\sqrt{uv}$ is real [Fig. 2(a)]. For H_{SSH}, it is slightly more complicated with $\bar{E}_{\mathrm{SSH}}=\pm\sqrt{1+t^2-\mu^2+2\sqrt{t^2-\mu^2}\cos k}$, which constitutes two mirror-imaged real line intervals if $t^2-\mu^2$ is real, and two curved hyperbola segments otherwise [Fig. 2(b)]. As such, the spectral graphs H_{HN} and H_{SSH} both correspond to the same dispersion class $P(E,z)=F(E)-(z+z^{-1})$, and are conformally related to each other.

(ii) $P(E,z)=F(E)-(z^a+z^{-b})$.

Next up is the dispersion class $F(E)=z^a+z^{-b}$, which is still separable, but without $z\to z^{-1}$ symmetry. It occurs when there are dissimilar hopping distances, such as in $H_{a,b}(z)=z^a+z^{-b}$, which contains hoppings of a/b sites to the left/right. A more sophisticated example would be $H^{\text{2-band}}_{2,1}(z)=(z^{-1}-1)\sigma_+ +(z+z^2-1)\sigma_-$, which corresponds to $F(E)=2-E^2$ and $a=2,b=1$, and is the one-dimensional (1D) precursor to a Chern model without Hermitian limit [68].

By considering simultaneous rotations of $F\to Fe^{i\theta}$, $z\to ze^{i\phi}$, it can be shown that $F(\bar{E})$ is a star with $(a+b)$-fold rotational symmetry [Fig. 2(c)]. Via a conformal transform, this star may be mapped into multiple distorted stars, such as $\bar{E}^{\text{2-band}}_{2,1}$ [Fig. 2(d)].

(iii) $P(E,z)=G(E)z+z^{-1}-F(E)$.

This dispersion class is nonseparable, containing a mixed term $G(E)z$ involving both E and z. It can arise from intra-sublattice hoppings in a multicomponent model, such as the minimal model with nontrivial trace

$$H_{\substack{F(E)=E^2,\\ G(E)=E}}(z)=\begin{pmatrix} rz & 1/z\\ 1 & 0\end{pmatrix}. \tag{2}$$

In general, mixed terms pose challenges in the analytic characterization of $\bar{E}$, because they make the GBZ notoriously difficult to express explicitly. However, for this specific ansatz $P(E,z)=G(E)z+z^{-1}-F(E)$, the OBC spectrum is exactly given by [69]

$$F(\bar{E})^2=\eta\,G(\bar{E}), \tag{3}$$

where $\eta\in\mathbb{R}$. This gives starlike spectral graphs when $F(E)$ and $G(E)$ are both monomials, but more esoteric looped topologies otherwise [Figs. 2(e), 2(f)]. Note that Hamiltonians corresponding to particular $F(E),G(E)$ are not unique, see Ref. [69] for more examples.

Classification of spectral graphs. We are now ready to analyze the spectral graph topology arising from more general energy dispersion, of the form

$$P(E,z)=Q(z)+r\,G(E)J(z)-F(E), \tag{4}$$

which involves not just the sum of z- and E-dependent terms, but also their product. Representative examples of such $P(E,z)$ are given in Table I. As shown shortly, their OBC spectral graphs depend intimately on their polynomial degrees $f=\deg[F(E)]$, $g=\deg[G(E)]$, $j=\deg[J(z)]$ and $q_\pm=\deg[Q(z^{\pm1})]$. Notably, r, the coefficient for the product term, can drive transitions between graph topologies; see the final section of the Supplemental Material [69] for an extensive array of examples.

While Eq. (4) admits no general analytical solution for its $\bar{E}$, we can comprehensively deduce its spectral graph structure by separately examining its small and large E limits. For definiteness, we specialize to

$$P(E,z)=z^{q_+}+\frac{1}{z^{q_-}}+r\,E^g z^j-E^f, \tag{5}$$

which is equivalent to many other realizations of Eq. (4) up to conformal transforms of E or rescalings of z.

When $E\to 0$, we have $P(E,z)\sim Q(z)+r\,G(E)J(z)=z^{q_+}+z^{-q_-}+rE^gz^j$, since $g<f=\dim(H)$ from the definition $P(E,z)=\mathrm{Det}[H(z)-\mathbb{I}\,E]$. Clearly, the condition $P(E,z)=0$ is equivalent to that of the previously discussed $P(E,z)=F(E)-(z^{q_+}+z^{-q_-})$, and we conclude that for small $|E|$, the OBC spectrum forms a star with

$$\mathcal{N}_S=f(q_+ + q_-) \tag{6}$$

rotationally symmetric branches centered at the origin. Note that since $Q(z)=\mathrm{Det}[H(z)]$, $\mathcal{N}_S$ is limited by $\max(q_+,q_-)\leqslant\dim(H)\mathrm{range}(H)$, where $\mathrm{range}(H)$ is the maximal hopping distance.

At sufficiently large $|E|$ and r, $P(E,z)\sim z^{q_\mp}+rE^gz^j-E^f$, where $\mp=-\mathrm{sgn}(j)$. By considering simultaneous phase rotations $E\to Ee^{i\theta}$, $z\to ze^{i\phi}$, one finds [69] that $\bar{E}$ is $2\pi/\mathcal{N}_L$ rotation symmetric, where

$$\mathcal{N}_L=\frac{(q_\mp+|j|)f-gq_\mp}{\mathrm{GCD}(q_\mp+|j|,q_\mp)}. \tag{7}$$

TABLE I. Different forms of the canonical dispersion $P(E, z)$ of Eq. (5) correspond to rich and diverse OBC spectral graphs $\bar{E}$. For each $P(E, z)$, we can (i) associate a nonunique minimal Hamiltonian $H(z)$; (ii) identify emergent global symmetries of $\bar{E}$ not necessary present in $H(z)$, and (iii) characterize its spectral graph topology with its number of branches $\mathcal{N}_S$, $\mathcal{N}_L$ and loops $\mathcal{N}_\ell$, as well as its adjacency matrix. See the Supplemental Material [69] for the latter as well as more examples with varying r.

	Char. Poly. $P(E,z)$	$\mathcal{N}_S$	$\mathcal{N}_L$	$\mathcal{N}_\ell$	Symmetry	Minimal Hamiltonian $H(z)$	Spectral graph e.g.
(i)	$z^2+1/z+r\ E\ z-E^2$	3	3	3	3-fold global, r-reflection	$\begin{pmatrix} rz & z^2+1/z \\ 1 & 0 \end{pmatrix}$	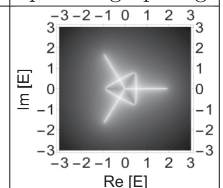
(ii)	$z^2+1/z+r\ E^2\ z-E^4$	6	6	6	6-fold global, reflection	$\begin{pmatrix} 0 & rz & 0 & z^2+1/z \\ 1 & 0 & 0 & 0 \\ 0 & 1 & 0 & 0 \\ 0 & 0 & 1 & 0 \end{pmatrix}$	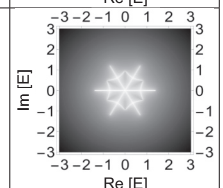
(iii)	$z^2+1/z+r\ E\ z-E^3$	3	5	0	None	$\begin{pmatrix} 0 & rz & z^2+1/z \\ 1 & 0 & 0 \\ 0 & 1 & 0 \end{pmatrix}$	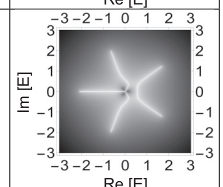
(iv)	$z^3+1/z^2+r\ E\ z-E^3$	5	7	Depends on r	None	$\begin{pmatrix} 0 & rz & z^3+1/z^2 \\ 1 & 0 & 0 \\ 0 & 1 & 0 \end{pmatrix}$	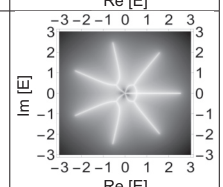
(v)	$z^2+1/z+r\ E^2\ z-E^3$	6	4	Depends on r	None	$\begin{pmatrix} rz & 0 & z^2+1/z \\ 1 & 0 & 0 \\ 0 & 1 & 0 \end{pmatrix}$	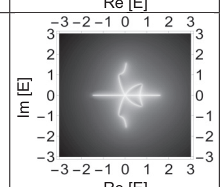
(vi)	$z^2+1/z+r\ E^3\ z-E^4$	9	5	3	r-reflection	$\begin{pmatrix} rz & 0 & 0 & z^2+1/z \\ 1 & 0 & 0 & 0 \\ 0 & 1 & 0 & 0 \\ 0 & 0 & 1 & 0 \end{pmatrix}$	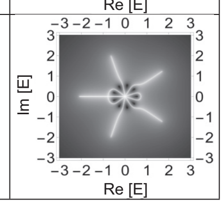

This emergent combination of $\mathcal{N}_S$- and $\mathcal{N}_L$-fold rotational symmetries can be employed for the design of new models with continua of real energy states [97], even when such symmetry is not obvious from the Hamiltonian.

Armed with Eqs. (6) and (7), one can deduce the topology of the entire spectral graph via the following heuristics:

(i) At small $|E|$ and large $|E|$, the OBC spectral graph of $P(E, z)$ have, respectively, $\mathcal{N}_S$ and $\mathcal{N}_L$ rotationally symmetric branches centered at the origin. The rest of the spectral graph interpolates between them.

(ii) Generally, the origin is the only branching point if $\mathcal{N}_L = \mathcal{N}_S$ [Table I (i)]. An exception might occur if the equal number of spectral branches at small and large $|E|$ are displaced by a small rotation angle. Additional branches appear to connect these two regimes, typically leading to a flowerlike shape [Table I (ii)].

(iii) When $\mathcal{N}_S < \mathcal{N}_L$, additional disjointed or isolated branches can appear at larger $|E|$ [Table I (iii)]. However, this condition alone does not guarantee the existence of isolated branches [Table I (iv) is connected].

(iv) Depending on the symmetry of $P(E, z)$ under $r \rightarrow -r$, the spectral graph at sufficiently large $\pm r$ are either identical, or mirror-reflected (r reflection).

(v) As we tune $|r|$, the number of rotationally symmetric branches interpolates between $\mathcal{N}_L$ at large $|r|$ and $f(q_+ + q_-)$ at small $|r|$, as exemplified in Ref. [69].

(vi) Sometimes, branches emanating from the origin may join up into loops. This is especially common when $\mathcal{N}_S > \mathcal{N}_L$ [Table I (v) and I (vi)], but may also appear when $\mathcal{N}_S < \mathcal{N}_L$ [Table I (iv)].

The total number of loops $\mathcal{N}_\ell$ is related to the number of vertices $\mathcal{V}$, branch segments $\mathcal{E}$ and disconnected spectral graph components $\mathcal{C}$ via Euler's formula on a planar graph [119]: $\mathcal{N}_\ell = \mathcal{C} + \mathcal{E} - \mathcal{V}$. Here $\mathcal{V}$ includes branching points as well as endpoints of branches; there are usually $\mathcal{N}_L$ of them, as showcased at the end of the Supplemental Material [69]. Consider Table I (iv), we have $\mathcal{V} = 13$, $\mathcal{E} = 14$, and $\mathcal{C} = 1$, and thus $\mathcal{N}_\ell = 1 + 13 - 11 = 2$ loops.

All in all, the graph structure is revealed through two different interpolations: that between small and large $|E|$ reveals the branching pattern for a particular $P(E, z)$ at large $|r|$, and further interpolating to $r = 0$ reveals additional topological transitions. Each of these branching points are spectral singularities, which lead to emergent complex flat bands [76]. For each graph, one may encode its topology by labeling its branching points and constructing the adjacency matrix [69].

Discussion. The proper understanding of the energy spectrum is central in explaining key response properties [120–122]. In particular, transitions in the spectral graph topology lead to emergent OBC flat bands [76,123–125], which are not only useful in sensing [77–80,126–128], but also physically result in responses kinks that can be measured in ultracold atomic settings [69]. Generalizing to two dimensions would potentially also give rise to interesting scenarios with discontinuous Berry curvature [68,81,82,84–86,129], particularly in nonlinear settings. In this work, we have uncovered that non-Hermitian spectra can present far richer graph topologies than hitherto reported, with their structure heuristically deducible from the dispersion equation $P(E, z)$ (Table I). The simplest topologies, i.e., the $P(E, z) = F(E) - (z + z^{-1})$ class have already been experimentally probed in ultracold atomic lattices [130–132] as well as photonic, mechanical, and electrical networks [17,26,107,133].

Mathematically, our characterization unveils new symmetries not present in the original Hamiltonian [69,101,105,134], and suggests new links between combinatorial graph theory, algebraic geometry[5] and non-Hermitian band topology [18,73,135,136]. One open mathematical question remains: For a given spectral graph topology, can one always find a local parent Hamiltonian?[6]

Moving forward, exciting discoveries are expected in the following directions: (i) Multidimensional generalizations, since the interplay with hybrid higher-order topology can lead to the spontaneous breaking of symmetries in the spectral graphs, as the κ deformation affects topological and bulk modes differently [90,137]. (ii) Introduction of interactions, which causes the aforementioned OBC flat bands to become highly susceptible to new many-body effects that are potentially accessible in ultracold atomic setups [132,138,139] and, more recently, quantum circuits [140–146] with monitored nonunitary measurements [147,148]. (iii) Quasiperiodicity will inevitably introduce self-similarity to the spectral graph topology [149], further enriching the classification.

Acknowledgments. T.T. is supported by the NSS scholarship by the Agency for Science, Technology and Research (A*STAR), Singapore. This work is supported by the Singapore National Research Foundation (Grant No. NRF2021-QEP2-02-P09).

[5]Our results are totally unrelated to known correspondences between polynomials and graphs, i.e., chromatic polynomials and Dessin d'enfants [152,153].

[6]A general construction exists by means of an electrostatic mapping [97], but locality is not guaranteed.

[1] F. Schindler, Z. Wang, M. G. Vergniory, A. M. Cook, A. Murani, S. Sengupta, A. Y. Kasumov, R. Deblock, S. Jeon, I. Drozdov, H. Bouchiat, S. Guéron, A. Yazdani, B. A. Bernevig, and T. Neupert, Higher-order topology in bismuth, Nature Phys. **14**, 918 (2018).
[2] H. Watanabe and H. C. Po, Fractional Corner Charge of Sodium Chloride, Phys. Rev. X **11**, 041064 (2021).
[3] F. D. M. Haldane and S. Raghu, Possible Realization of Directional Optical Waveguides in Photonic Crystals with Broken Time-Reversal Symmetry, Phys. Rev. Lett. **100**, 013904 (2008).
[4] Z. Wang, Y. Chong, J. Joannopoulos, and M. Soljačić, Observation of unidirectional backscattering-immune topological electromagnetic states, Nature (London) **461**, 772 (2009).
[5] L. Lu, L. Fu, J. D. Joannopoulos, and M. Soljačić, Weyl points and line nodes in gyroid photonic crystals, Nature Photon. **7**, 294 (2013).
[6] L. Lu, J. D. Joannopoulos, and M. Soljačić, Topological photonics, Nature Photon. **8**, 821 (2014).
[7] J. Y. Lin, N. C. Hu, Y. J. Chen, C. H. Lee, and X. Zhang, Line nodes, dirac points, and lifshitz transition in two-dimensional nonsymmorphic photonic crystals, Phys. Rev. B **96**, 075438 (2017).
[8] B.-Y. Xie, H.-F. Wang, H.-X. Wang, X.-Y. Zhu, J.-H. Jiang, M.-H. Lu, and Y.-F. Chen, Second-order photonic topological insulator with corner states, Phys. Rev. B **98**, 205147 (2018).
[9] K. Ding, G. Ma, M. Xiao, Z. Q. Zhang, and C. T. Chan, Emergence, Coalescence, and Topological Properties of Multiple Exceptional Points and Their Experimental Realization, Phys. Rev. X **6**, 021007 (2016).
[10] S. Klembt, T. Harder, O. Egorov, K. Winkler, R. Ge, M. Bandres, M. Emmerling, L. Worschech, T. Liew, M. Segev *et al.*, Exciton-polariton topological insulator, Nature (London) **562**, 552 (2018).
[11] W. Song, W. Sun, C. Chen, Q. Song, S. Xiao, S. Zhu, and T. Li, Breakup and Recovery of Topological Zero Modes in Finite Non-Hermitian Optical Lattices, Phys. Rev. Lett. **123**, 165701 (2019).
[12] X. Zhu, H. Wang, S. K. Gupta, H. Zhang, B. Xie, M. Lu, and Y. Chen, Photonic non-hermitian skin effect and non-bloch bulk-boundary correspondence, Phys. Rev. Res. **2**, 013280 (2020).
[13] C. Kane and T. Lubensky, Topological boundary modes in isostatic lattices, Nature Phys. **10**, 39 (2014).
[14] V. Peano, C. Brendel, M. Schmidt, and F. Marquardt, Topological Phases of Sound and Light, Phys. Rev. X **5**, 031011 (2015).

[15] R. Süsstrunk and S. D. Huber, Observation of phononic helical edge states in a mechanical topological insulator, Science **349**, 47 (2015).

[16] L. M. Nash, D. Kleckner, A. Read, V. Vitelli, A. M. Turner, and W. T. Irvine, Topological mechanics of gyroscopic metamaterials, Proc. Natl. Acad. Sci. USA **112**, 14495 (2015).

[17] A. Ghatak, M. Brandenbourger, J. van Wezel, and C. Coulais, Observation of non-Hermitian topology and its bulk–edge correspondence in an active mechanical metamaterial, Proc. Natl. Acad. Sci. USA **117**, 29561 (2020).

[18] C. Scheibner, W. T. M. Irvine, and V. Vitelli, Non-Hermitian Band Topology and Skin Modes in Active Elastic Media, Phys. Rev. Lett. **125**, 118001 (2020).

[19] J. Hou, Z. Li, X.-W. Luo, Q. Gu, and C. Zhang, Topological Bands and Triply Degenerate Points in Non-Hermitian Hyperbolic Metamaterials, Phys. Rev. Lett. **124**, 073603 (2020).

[20] J. Ningyuan, C. Owens, A. Sommer, D. Schuster, and J. Simon, Time- and Site-Resolved Dynamics in a Topological Circuit, Phys. Rev. X **5**, 021031 (2015).

[21] S. Imhof, C. Berger, F. Bayer, J. Brehm, L. W. Molenkamp, T. Kiessling, F. Schindler, C. H. Lee, M. Greiter, T. Neupert *et al.*, Topolectrical-circuit realization of topological corner modes, Nature Phys. **14**, 925 (2018).

[22] T. Hofmann, T. Helbig, C. H. Lee, M. Greiter, and R. Thomale, Chiral Voltage Propagation and Calibration in a Topolectrical Chern Circuit, Phys. Rev. Lett. **122**, 247702 (2019).

[23] Y. Wang, H. M. Price, B. Zhang, and Y. Chong, Circuit implementation of a four-dimensional topological insulator, Nature Commun. **11**, 2356 (2020).

[24] L. Li, C. H. Lee, and J. Gong, Emergence and full 3d-imaging of nodal boundary seifert surfaces in 4d topological matter, Commun. Phys. **2**, 135 (2019).

[25] N. A. Olekhno, E. I. Kretov, A. A. Stepanenko, P. A. Ivanova, V. V. Yaroshenko, E. M. Puhtina, D. S. Filonov, B. Cappello, L. Matekovits, and M. A. Gorlach, Topological edge states of interacting photon pairs emulated in a topolectrical circuit, Nature Commun. **11**, 1436 (2020).

[26] T. Helbig, T. Hofmann, S. Imhof, M. Abdelghany, T. Kiessling, L. Molenkamp, C. Lee, A. Szameit, M. Greiter, and R. Thomale, Generalized bulk–boundary correspondence in non-hermitian topolectrical circuits, Nature Phys. **16**, 747 (2020).

[27] D. Zou, T. Chen, W. He, J. Bao, C. H. Lee, H. Sun, and X. Zhang, Observation of hybrid higher-order skin-topological effect in non-Hermitian topolectrical circuits, Nature Commun. **12**, 7201 (2021).

[28] A. Stegmaier, S. Imhof, T. Helbig, T. Hofmann, C. H. Lee, M. Kremer, A. Fritzsche, T. Feichtner, S. Klembt, S. Höfling, I. Boettcher, I. C. Fulga, L. Ma, O. G. Schmidt, M. Greiter, T. Kiessling, A. Szameit, and R. Thomale, Topological Defect Engineering and $\mathcal{PT}$ Symmetry in Non-Hermitian Electrical Circuits, Phys. Rev. Lett. **126**, 215302 (2021).

[29] P. M. Lenggenhager, A. Stegmaier, L. K. Upreti, T. Hofmann, T. Helbig, A. Vollhardt, M. Greiter, C. H. Lee, S. Imhof, H. Brand *et al.*, Simulating hyperbolic space on a circuit board, Nature Commun. **13**, 4373 (2022).

[30] Y. Yang, D. Zhu, Z. Hang, and Y. Chong, Observation of antichiral edge states in a circuit lattice, Sci. China Phys. Mech. Astron. **64**, 257011 (2021).

[31] X. Zhang, B. Zhang, W. Zhao, and C. H. Lee, Observation of non-local impedance response in a passive electrical circuit, arXiv:2211.09152.

[32] C. Shang, S. Liu, R. Shao, P. Han, X. Zang, X. Zhang, K. N. Salama, W. Gao, C. H. Lee, R. Thomale *et al.*, Experimental identification of the second-order non-hermitian skin effect with physics-graph-informed machine learning, Adv. Sci. **9**, 2202922 (2022).

[33] H. Hohmann, T. Hofmann, T. Helbig, S. Imhof, H. Brand, L. K. Upreti, A. Stegmaier, A. Fritzsche, T. Müller, U. Schwingenschlögl *et al.*, Observation of cnoidal wave localization in nonlinear topolectric circuits, Phys. Rev. Res. **5**, L012041 (2023).

[34] P. Zhu, X.-Q. Sun, T. L. Hughes, and G. Bahl, Higher rank chirality and non-hermitian skin effect in a topolectrical circuit, Nature Commun. **14**, 720 (2023).

[35] H. Zhang, T. Chen, L. Li, C. H. Lee, and X. Zhang, Electrical circuit realization of topological switching for the non-hermitian skin effect, Phys. Rev. B **107**, 085426 (2023).

[36] C. L. Kane and E. J. Mele, Quantum Spin Hall Effect in Graphene, Phys. Rev. Lett. **95**, 226801 (2005).

[37] C. L. Kane and E. J. Mele, Z_2 Topological Order and the Quantum Spin Hall Effect, Phys. Rev. Lett. **95**, 146802 (2005).

[38] M. König, S. Wiedmann, C. Brüne, A. Roth, H. Buhmann, L. W. Molenkamp, X.-L. Qi, and S.-C. Zhang, Quantum spin hall insulator state in hgte quantum wells, Science **318**, 766 (2007).

[39] L. Fu, C. L. Kane, and E. J. Mele, Topological Insulators in Three Dimensions, Phys. Rev. Lett. **98**, 106803 (2007).

[40] L. Fu and C. L. Kane, Topological insulators with inversion symmetry, Phys. Rev. B **76**, 045302 (2007).

[41] J. Moore, Topological insulators: The next generation, Nature Phys. **5**, 378 (2009).

[42] Y. Gu, C. H. Lee, X. Wen, G. Y. Cho, S. Ryu, and X.-L. Qi, Holographic duality between (2+ 1)-dimensional quantum anomalous hall state and (3+ 1)-dimensional topological insulators, Phys. Rev. B **94**, 125107 (2016).

[43] M. Z. Hasan and C. L. Kane, Colloquium: topological insulators, Rev. Mod. Phys. **82**, 3045 (2010).

[44] F. Schindler, A. M. Cook, M. G. Vergniory, Z. Wang, S. S. P. Parkin, B. A. Bernevig, and T. Neupert, Higher-order topological insulators, Sci. Adv. **4**, eaat0346 (2018).

[45] W. A. Benalcazar, B. A. Bernevig, and T. L. Hughes, Quantized electric multipole insulators, Science **357**, 61 (2017).

[46] Z. Song, Z. Fang, and C. Fang, $(d-2)$-Dimensional Edge States of Rotation Symmetry Protected Topological States, Phys. Rev. Lett. **119**, 246402 (2017).

[47] S. Franca, J. van den Brink, and I. C. Fulga, An anomalous higher-order topological insulator, Phys. Rev. B **98**, 201114(R) (2018).

[48] E. Edvardsson, F. K. Kunst, and E. J. Bergholtz, Non-hermitian extensions of higher-order topological phases and their biorthogonal bulk-boundary correspondence, Phys. Rev. B **99**, 081302(R) (2019).

[49] B. I. Halperin, Quantized hall conductance, current-carrying edge states, and the existence of extended states in a

two-dimensional disordered potential, Phys. Rev. B **25**, 2185 (1982).

[50] A. H. MacDonald and P. Středa, Quantized hall effect and edge currents, Phys. Rev. B **29**, 1616 (1984).

[51] F. D. M. Haldane, Model for a Quantum Hall Effect without Landau Levels: Condensed-Matter Realization of the "Parity Anomaly", Phys. Rev. Lett. **61**, 2015 (1988).

[52] C.-X. Liu, S.-C. Zhang, and X.-L. Qi, The quantum anomalous hall effect: Theory and experiment, Annu. Rev. Condens. Matter Phys. **7**, 301 (2016).

[53] W. Heiss, The physics of exceptional points, J. Phys. A: Math. Theor. **45**, 444016 (2012).

[54] B. Zhen, C. W. Hsu, Y. Igarashi, L. Lu, I. Kaminer, A. Pick, S.-L. Chua, J. D. Joannopoulos, and M. Soljačić, Spawning rings of exceptional points out of dirac cones, Nature (London) **525**, 354 (2015).

[55] A. U. Hassan, B. Zhen, M. Soljačić, M. Khajavikhan, and D. N. Christodoulides, Dynamically Encircling Exceptional Points: Exact Evolution and Polarization State Conversion, Phys. Rev. Lett. **118**, 093002 (2017).

[56] H. Hodaei, A. U. Hassan, S. Wittek, H. Garcia-Gracia, R. El-Ganainy, D. N. Christodoulides, and M. Khajavikhan, Enhanced sensitivity at higher-order exceptional points, Nature (London) **548**, 187 (2017).

[57] W. Hu, H. Wang, P. P. Shum, and Y. D. Chong, Exceptional points in a non-hermitian topological pump, Phys. Rev. B **95**, 184306 (2017).

[58] T. Gao, G. Li, E. Estrecho, T. C. H. Liew, D. Comber-Todd, A. Nalitov, M. Steger, K. West, L. Pfeiffer, D. W. Snoke, A. V. Kavokin, A. G. Truscott, and E. A. Ostrovskaya, Chiral Modes at Exceptional Points in Exciton-Polariton Quantum Fluids, Phys. Rev. Lett. **120**, 065301 (2018).

[59] X.-L. Zhang, S. Wang, B. Hou, and C. T. Chan, Dynamically Encircling Exceptional Points: In situ Control of Encircling Loops and the Role of the Starting Point, Phys. Rev. X **8**, 021066 (2018).

[60] H. Zhou, C. Peng, Y. Yoon, C. W. Hsu, K. A. Nelson, L. Fu, J. D. Joannopoulos, M. Soljačić, and B. Zhen, Observation of bulk fermi arc and polarization half charge from paired exceptional points, Science **359**, 1009 (2018).

[61] L. Jin, H. C. Wu, B.-B. Wei, and Z. Song, Hybrid exceptional point created from type-III dirac point, Phys. Rev. B **101**, 045130 (2020).

[62] B. Dóra, M. Heyl, and R. Moessner, The kibble-zurek mechanism at exceptional points, Nature Commun. **10**, 2254 (2019).

[63] M. M. Denner, A. Skurativska, F. Schindler, M. H. Fischer, R. Thomale, T. Bzdušek, and T. Neupert, Exceptional topological insulators, Nature Commun. **12**, 5681 (2021).

[64] C. H. Lee, Exceptional Bound States and Negative Entanglement Entropy, Phys. Rev. Lett. **128**, 010402 (2022).

[65] T. Yoshida and Y. Hatsugai, Exceptional rings protected by emergent symmetry for mechanical systems, Phys. Rev. B **100**, 054109 (2019).

[66] O. Giménez and M. Noy, Asymptotic enumeration and limit laws of planar graphs, J. Amer. Math. Soc. **22**, 309 (2009).

[67] L. Li, C. H. Lee, S. Mu, and J. Gong, Critical non-hermitian skin effect, Nature Commun. **11**, 5491 (2020).

[68] C. H. Lee, L. Li, R. Thomale, and J. Gong, Unraveling non-hermitian pumping: Emergent spectral singularities and anomalous responses, Phys. Rev. B **102**, 085151 (2020).

[69] See Supplemental Material at http://link.aps.org/supplemental/10.1103/PhysRevB.107.L220301 for adjacency matrix as well as more examples with varying r.

[70] C. H. Lee and R. Thomale, Anatomy of skin modes and topology in non-hermitian systems, Phys. Rev. B **99**, 201103(R) (2019).

[71] Z. Yang, K. Zhang, C. Fang, and J. Hu, Non-Hermitian Bulk-Boundary Correspondence and Auxiliary Generalized Brillouin Zone Theory, Phys. Rev. Lett. **125**, 226402 (2020).

[72] S. Yao and Z. Wang, Edge States and Topological Invariants of Non-Hermitian Systems, Phys. Rev. Lett. **121**, 086803 (2018).

[73] X. Zhang, G. Li, Y. Liu, T. Tai, R. Thomale, and C. H. Lee, Tidal surface states as fingerprints of non-hermitian nodal knot metals, Commun. Phys. **4**, 47 (2021).

[74] N. Hatano and D. R. Nelson, Localization Transitions in Non-Hermitian Quantum Mechanics, Phys. Rev. Lett. **77**, 570 (1996).

[75] N. Hatano and D. R. Nelson, Non-Hermitian delocalization and eigenfunctions, Phys. Rev. B **58**, 8384 (1998).

[76] C. H. Lee, D. P. Arovas, and R. Thomale, Band flatness optimization through complex analysis, Phys. Rev. B **93**, 155155 (2016).

[77] J. C. Budich and E. J. Bergholtz, Non-Hermitian Topological Sensors, Phys. Rev. Lett. **125**, 180403 (2020).

[78] J. Wiersig, Prospects and fundamental limits in exceptional point-based sensing, Nature Commun. **11**, 2454 (2020).

[79] H.-K. Lau and A. A. Clerk, Fundamental limits and nonreciprocal approaches in non-Hermitian quantum sensing, Nature Commun. **9**, 4320 (2018).

[80] M. Zhang, W. Sweeney, C. W. Hsu, L. Yang, A. D. Stone, and L. Jiang, Quantum Noise Theory of Exceptional Point Amplifying Sensors, Phys. Rev. Lett. **123**, 180501 (2019).

[81] D. Xiao, M.-C. Chang, and Q. Niu, Berry phase effects on electronic properties, Rev. Mod. Phys. **82**, 1959 (2010).

[82] T. Morimoto and N. Nagaosa, Topological nature of nonlinear optical effects in solids, Sci. Adv. **2**, e1501524 (2016).

[83] C. H. Lee, H. H. Yap, T. Tai, G. Xu, X. Zhang, and J. Gong, Enhanced higher harmonic generation from nodal topology, Phys. Rev. B **102**, 035138 (2020).

[84] L. Zhang, Berry curvature and various thermal hall effects, New J. Phys. **18**, 103039 (2016).

[85] V. Cvetkovic and O. Vafek, Berry phases and the intrinsic thermal hall effect in high-temperature cuprate superconductors, Nature Commun. **6**, 6518 (2015).

[86] Y. P. Mizuta and F. Ishii, Contribution of berry curvature to thermoelectric effects, JPS Conf. Proc. **3**, 017035 (2014).

[87] F. Song, S. Yao, and Z. Wang, Non-Hermitian Topological Invariants in Real Space, Phys. Rev. Lett. **123**, 246801 (2019).

[88] N. W. Ashcroft and N. D. Mermin, *Solid State Physics* (Saunders College, Philadelphia, 1976).

[89] H. M. Price and N. R. Cooper, Mapping the berry curvature from semiclassical dynamics in optical lattices, Phys. Rev. A **85**, 033620 (2012).

[90] C. H. Lee, L. Li, and J. Gong, Hybrid Higher-Order Skin-Topological Modes in Nonreciprocal Systems, Phys. Rev. Lett. **123**, 016805 (2019).

[91] C. M. Bender and S. Boettcher, Real Spectra in Non-Hermitian Hamiltonians Having PT Symmetry, Phys. Rev. Lett. **80**, 5243 (1998).

[92] T. Ozawa, H. M. Price, A. Amo, N. Goldman, M. Hafezi, L. Lu, M. C. Rechtsman, D. Schuster, J. Simon, O. Zilberberg, and I. Carusotto, Topological photonics, Rev. Mod. Phys. **91**, 015006 (2019).

[93] L. Feng, R. El-Ganainy, and L. Ge, Non-hermitian photonics based on parity–time symmetry, Nature Photon. **11**, 752 (2017).

[94] R. El-Ganainy, K. G. Makris, M. Khajavikhan, Z. H. Musslimani, S. Rotter, and D. N. Christodoulides, Non-Hermitian physics and PT symmetry, Nature Phys. **14**, 11 (2018).

[95] S. Longhi, Non-Bloch-Band Collapse and Chiral Zener Tunneling, Phys. Rev. Lett. **124**, 066602 (2020).

[96] Y. Long, H. Xue, and B. Zhang, Non-Hermitian topological systems with eigenvalues that are always real, Phys. Rev. B **105**, L100102 (2022).

[97] R. Yang, J. W. Tan, T. Tai, J. M. Koh, L. Li, S. Longhi, and C. H. Lee, Designing non-hermitian real spectra through electrostatics, Sci. Bull. **67**, 1865 (2022).

[98] H. Jiang and C. H. Lee, Dimensional transmutation from non-Hermiticity, arXiv:2207.08843.

[99] K. Yokomizo and S. Murakami, Non-Bloch Band Theory of Non-Hermitian Systems, Phys. Rev. Lett. **123**, 066404 (2019).

[100] T. E. Lee, Anomalous Edge State in a non-Hermitian Lattice, Phys. Rev. Lett. **116**, 133903 (2016).

[101] Z. Gong, Y. Ashida, K. Kawabata, K. Takasan, S. Higashikawa, and M. Ueda, Topological Phases of Non-Hermitian Systems, Phys. Rev. X **8**, 031079 (2018).

[102] H. Schomerus, Nonreciprocal response theory of non-Hermitian mechanical metamaterials: Response phase transition from the skin effect of zero modes, Phys. Rev. Res. **2**, 013058 (2020).

[103] D. S. Borgnia, A. J. Kruchkov, and R.-J. Slager, Non-Hermitian Boundary Modes and Topology, Phys. Rev. Lett. **124**, 056802 (2020).

[104] K. Zhang, Z. Yang, and C. Fang, Correspondence between Winding Numbers and Skin Modes in Non-Hermitian Systems, Phys. Rev. Lett. **125**, 126402 (2020).

[105] N. Okuma, K. Kawabata, K. Shiozaki, and M. Sato, Topological Origin of Non-Hermitian Skin Effects, Phys. Rev. Lett. **124**, 086801 (2020).

[106] K. Kawabata, M. Sato, and K. Shiozaki, Higher-order non-Hermitian skin effect, Phys. Rev. B **102**, 205118 (2020).

[107] L. Xiao, T. Deng, K. Wang, G. Zhu, Z. Wang, W. Yi, and P. Xue, Non-Hermitian bulk–boundary correspondence in quantum dynamics, Nature Phys. **16**, 761 (2020).

[108] W.-T. Xue, M.-R. Li, Y.-M. Hu, F. Song, and Z. Wang, Simple formulas of directional amplification from non-bloch band theory, Phys. Rev. B **103**, L241408 (2021).

[109] S. Mu, C. H. Lee, L. Li, and J. Gong, Emergent fermi surface in a many-body non-Hermitian fermionic chain, Phys. Rev. B **102**, 081115(R) (2020).

[110] M. I. Rosa and M. Ruzzene, Dynamics and topology of non-hermitian elastic lattices with non-local feedback control interactions, New J. Phys. **22**, 053004 (2020).

[111] C. H. Lee and S. Longhi, Ultrafast and anharmonic rabi oscillations between non-bloch bands, Commun. Phys. **3**, 147 (2020).

[112] C. H. Lee, Many-body topological and skin states without open boundaries, Phys. Rev. B **104**, 195102 (2021).

[113] L. Li, C. H. Lee, and J. Gong, Impurity induced scale-free localization, Commun. Phys. **4**, 42 (2021).

[114] R. Shen and C. H. Lee, Non-Hermitian skin clusters from strong interactions, Commun. Phys. **5**, 238 (2022).

[115] H. Jiang and C. H. Lee, Filling up complex spectral regions through non-hermitian disordered chains, Chin. Phys. B **31**, 050307 (2022).

[116] C. H. Lee and P. Ye, Free-fermion entanglement spectrum through wannier interpolation, Phys. Rev. B **91**, 085119 (2015).

[117] R. Lin, T. Tai, L. Li, and C. H. Lee, Topological non-Hermitian skin effect, arXiv:2302.03057.

[118] P. Roth, *Arithmetica philosophica, oder schöne newe wolgegründte überauß künstliche Rechnung der Coß oder Algebrae: in drey unterschiedliche Theil getheilt*, (Verlag des Authoris)

[119] L. Euler, Elementa doctrinae solidorum, Novi commentarii academiae scientiarum Petropolitanae **4**, 109 (1758).

[120] A. Zanatta, Revisiting the optical bandgap of semiconductors and the proposal of a unified methodology to its determination, Sci. Rep. **9**, 11225 (2019).

[121] A. Chaves, J. Azadani, H. Alsalman, D. Da Costa, R. Frisenda, A. Chaves, S. H. Song, Y. Kim, D. He, J. Zhou *et al.*, Bandgap engineering of two-dimensional semiconductor materials, npj 2D Mater. Appl. **4**, 29 (2020).

[122] M. Bernardi, C. Ataca, M. Palummo, and J. C. Grossman, Optical and electronic properties of two-dimensional layered materials, Nanophoton. **6**, 479 (2017).

[123] V. M. Martinez Alvarez, J. E. Barrios Vargas, and L. E. F. Foa Torres, Non-Hermitian robust edge states in one dimension: Anomalous localization and eigenspace condensation at exceptional points, Phys. Rev. B **97**, 121401(R) (2018).

[124] L. Chen, T. Mazaheri, A. Seidel, and X. Tang, The impossibility of exactly flat non-trivial chern bands in strictly local periodic tight binding models, J. Phys. A: Math. Theor. **47**, 152001 (2014).

[125] C. H. Lee and X.-L. Qi, Lattice construction of pseudopotential hamiltonians for fractional chern insulators, Phys. Rev. B **90**, 085103 (2014).

[126] Y.-Y. Zou, Y. Zhou, L.-M. Chen, and P. Ye, Detecting bulk and edge exceptional points in non-Hermitian systems through generalized Petermann factors, arXiv:2208.14944.

[127] J. Wiersig, Petermann factors and phase rigidities near exceptional points, arXiv:2304.00764.

[128] W. Ding, X. Wang, and S. Chen, Fundamental sensitivity limits for non-Hermitian quantum sensors, arXiv:2304.08374.

[129] T. Tuloup, R. W. Bomantara, C. H. Lee, and J. Gong, Nonlinearity induced topological physics in momentum space and real space, Phys. Rev. B **102**, 115411 (2020).

[130] W. Gou, T. Chen, D. Xie, T. Xiao, T.-S. Deng, B. Gadway, W. Yi, and B. Yan, Tunable Nonreciprocal Quantum Transport through a Dissipative Aharonov-Bohm Ring in Ultracold Atoms, Phys. Rev. Lett. **124**, 070402 (2020).

[131] D. P. Pires and T. Macrì, Probing phase transitions in non-Hermitian systems with multiple quantum coherences, Phys. Rev. B **104**, 155141 (2021).

[132] Q. Liang, D. Xie, Z. Dong, H. Li, H. Li, B. Gadway, W. Yi, and B. Yan, Dynamic Signatures of Non-Hermitian Skin Effect and Topology in Ultracold Atoms, Phys. Rev. Lett. **129**, 070401 (2022).
[133] S. Weidemann, M. Kremer, T. Helbig, T. Hofmann, A. Stegmaier, M. Greiter, R. Thomale, and A. Szameit, Topological funneling of light, Science **368**, 311 (2020).
[134] K. Kawabata, K. Shiozaki, M. Ueda, and M. Sato, Symmetry and Topology in Non-Hermitian Physics, Phys. Rev. X **9**, 041015 (2019).
[135] R. Okugawa, R. Takahashi, and K. Yokomizo, Non-Hermitian band topology with generalized inversion symmetry, Phys. Rev. B **103**, 205205 (2021).
[136] L. Li and C. H. Lee, Non-Hermitian pseudo-gaps, Sci. Bull. **67**, 685 (2022).
[137] Z. Lei, C. H. Lee, and L. Li, PT-activated non-Hermitian skin modes, arXiv:2304.13955.
[138] H. Bernien, S. Schwartz, A. Keesling, H. Levine, A. Omran, H. Pichler, S. Choi, A. S. Zibrov, M. Endres, M. Greiner, V. Vuletić, and M. D. Lukin, Probing many-body dynamics on a 51-atom quantum simulator, Nature (London) **551**, 579 (2017).
[139] L. Li, C. H. Lee, and J. Gong, Topological Switch for Non-Hermitian Skin Effect in Cold-Atom Systems with Loss, Phys. Rev. Lett. **124**, 250402 (2020).
[140] K. Choo, C. W. von Keyserlingk, N. Regnault, and T. Neupert, Measurement of the Entanglement Spectrum of a Symmetry-Protected Topological State using the IBM Quantum Computer, Phys. Rev. Lett. **121**, 086808 (2018).
[141] A. Smith, B. Jobst, A. G. Green, and F. Pollmann, Crossing a topological phase transition with a quantum computer, Phys. Rev. Res. **4**, L022020 (2022).
[142] D. Azses, R. Haenel, Y. Naveh, R. Raussendorf, E. Sela, and E. G. Dalla Torre, Identification of Symmetry-Protected Topological States on Noisy Quantum Computers, Phys. Rev. Lett. **125**, 120502 (2020).
[143] F. Mei, Q. Guo, Y.-F. Yu, L. Xiao, S.-L. Zhu, and S. Jia, Digital Simulation of Topological Matter on Programmable Quantum Processors, Phys. Rev. Lett. **125**, 160503 (2020).
[144] J. M. Koh, T. Tai, Y. H. Phee, W. E. Ng, and C. H. Lee, Stabilizing multiple topological fermions on a quantum computer, npj Quantum Inf. **8**, 16 (2022).
[145] J. M. Koh, T. Tai, and C. H. Lee, Simulation of Interaction-Induced Chiral Topological Dynamics on a Digital Quantum Computer, Phys. Rev. Lett. **129**, 140502 (2022).
[146] J. M. Koh, T. Tai, and C. H. Lee, Observation of higher-order topological states on a quantum computer, arXiv:2303.02179.
[147] S. Dogra, A. A. Melnikov, and G. S. Paraoanu, Quantum simulation of parity–time symmetry breaking with a superconducting quantum processor, Commun. Phys. **4**, 26 (2021).
[148] C. Fleckenstein, A. Zorzato, D. Varjas, E. J. Bergholtz, J. H. Bardarson, and A. Tiwari, Non-Hermitian topology in monitored quantum circuits, Phys. Rev. Res. **4**, L032026 (2022).
[149] S. Manna and B. Roy, Inner skin effects on non-hermitian topological fractals, Commun. Phys. **6**, 10 (2023).
[150] L. Li, S. Mu, C. H. Lee, and J. Gong, Quantized classical response from spectral winding topology, Nature Commun. **12**, 5294 (2021).
[151] P. Ruffini, *Riflessioni intorno alla soluzione delle equazioni algebraiche generali opuscolo del cav. dott. Paolo Ruffini.* (presso la Societa Tipografica, 1813).
[152] G. Jones, Dessins d'enfants: Bipartite maps and galois groups, Séminaire Lotharingien de Combinatoire [electronic only] **35**, B35d (1995).
[153] R. C. Read, An introduction to chromatic polynomials, J. Combin. Theory **4**, 52 (1968).